THE X-RAY LUMINOSITY−MASS RELATION FOR LOCAL CLUSTERS OF GALAXIES

R. STANEK[1,5], A.E. EVRARD[1,2,3], H. BÖHRINGER[4], P. SCHUECKER[4], B. NORD[2]
Draft version February 5, 2008

ABSTRACT

We investigate the relationship between soft X-ray luminosity and mass for low redshift clusters of galaxies by comparing observed number counts and scaling laws to halo-based expectations of ΛCDM cosmologies. We model the conditional likelihood of halo luminosity as a log-normal distributon of fixed width, centered on a scaling relation, $L \propto M^p \rho_c{}^s(z)$, and consider two values for s, appropriate for self-similar evolution or no evolution. Convolving with the halo mass function, we compute expected counts in redshift and flux which, after appropriate survey effects are included, we compare to REFLEX survey data. Counts alone provide only an upper limit on the scatter in mass at fixed luminosity, $\sigma_{\ln M} < 0.4$. We argue that the observed, intrinsic variance in the temperature–luminosity relation is directly indicative of mass–luminosity variance, and derive $\sigma_{\ln M} = 0.43 \pm 0.06$ from HIFLUGCS data. When added to the likelihood analysis, we derive values $p = 1.59 \pm 0.05$, $\ln L_{15,0} = 1.34 \pm 0.09$, and $\sigma_{\ln M} = 0.37 \pm 0.05$ for self-similar redshift evolution in a concordance ($\Omega_m = 0.3$, $\Omega_\Lambda = 0.7$, $\sigma_8 = 0.9$) universe. The present-epoch intercept is sensitive to power spectrum normalization, $L_{15,0} \propto \sigma_8{}^{-4}$, and the slope is weakly sensitive to the matter density, $p \propto \Omega_m^{1/2}$. We find a substantially (factor 2) dimmer intercept and slightly steeper slope than the values published using hydrostatic mass estimates of the HIFLUGCS sample, and show that a Malmquist bias of the X-ray flux-limited sample accounts for this effect. In light of new WMAP constraints, we discuss the interplay between parameters and sources of systematic error, and offer a compromise model with $\Omega_m = 0.24$, $\sigma_8 = 0.85$, and somewhat lower scatter $\sigma_{\ln M} = 0.25$, in which hydrostatic mass estimates remain accurate to $\sim 15\%$. We stress the need for independent calibration of the L-M relation via weak gravitational lensing.

Subject headings: clusters: general — clusters: ICM — clusters: cosmology— X-rays: clusters

1. INTRODUCTION

The counts, spatial clustering and bulk properties of the most massive halos in the universe offer a means to test cosmological physics (Wang & Steinhardt 1998; Haiman et al. 2001; Carlstrom et al. 2002; Majumdar & Mohr 2003; Battye & Weller 2003; Wang et al. 2004). Although only a handful of high redshift ($z \gtrsim 1$) clusters are currently known, the number will grow considerably in the next five years, as a result of improved search techniques using multi-band optical (Gladders & Yee 2005) combined with infrared (Stanford et al. 2005) or X-ray (Rosati et al. 1998; Romer et al. 2000; Mullis et al. 2005) imaging. Sunyaev-Zel'dovich (SZ) surveys, based on interferometric (Holder et al. 2000; Loh et al. 2005), or bolometric (Schwan et al. 2003; Kosowsky 2003; Ruhl et al. 2004) approaches, will ultimately extend the reach of the cluster population to $z \sim 3$.

Since observational surveys do not select directly on halo mass, interpreting the data requires a model that relates observable bulk features, such as temperature, Sunyaev-Zel'dovich decrement, or X-ray luminosity, to mass. Given sufficiently rich cluster samples, one can solve for parameters describing the mass-observable relation along with cosmological parameters in a simultaneous fashion (Levine et al. 2002; Majumdar & Mohr 2003; Lima & Hu 2004). Power-law relationships between bulk properties are expected on dimensional grounds (Kaiser 1986), but the scatter about mean mass-observable relationships, a crucial element of self-calibration exercises (Levine et al. 2002; Lima & Hu 2005), is presently poorly understood.

In this paper, we use counts and scaling relations of low redshift clusters in the HIFLUGCS survey (Reiprich & Böhringer 2002) to investigate the statistical relationship between X-ray luminosity and total halo mass. The method relies on numerical simulations for calibration of the space density of massive halos (Sheth & Tormen 1999; Reed et al. 2003; Jenkins et al. 2001; Warren et al. 2005) and for an estimate of the covariance of X-ray temperature and luminosity at fixed mass.

For a set of structurally identical, spherical halos with mass M_Δ, radius R_Δ (here Δ is a threshold defining the halo edge relative to the critical density) and with intracluster gas fraction $f_{\rm ICM} = M_{\rm ICM}/M_\Delta$, one expects the bolometric luminosity to scale as (Arnaud & Evrard 1999)

$$L_{\rm bol}(M,z) \;=\; C\,Q_L\,f_{\rm ICM}^2\,\rho_c^{7/6}(z)\,M_\Delta^{4/3}, \tag{1}$$

[1] Department of Astronomy and Michigan Center for Theoretical Physics, University of Michigan, 500 Church St., Ann Arbor, MI 48109
[2] Department of Physics and Michigan Center for Theoretical Physics, University of Michigan, 450 Church St., Ann Arbor, MI 48109-1040
[3] Visiting Miller Professor, Physics Department, University of California, Berkeley, CA 94720
[4] Max-Planck-Institut für extraterrestrische Physik, D-85740 Garching, Germany
[5] email: rstanek@umich.edu

where C is a constant, $\rho_c(z)$ is the critical density, and $Q_L = (3/4\pi) \int d^3y g^2(y)$ is a structure function that is sensitive to the second moment of the normalized gas density profile

$$\rho_{\rm ICM}(r) = f_{\rm ICM} \Delta \rho_c(z)\, g(r/R_\Delta). \tag{2}$$

If the ensemble average gas fraction or radial structure function vary with mass and epoch, then the power law exponents will generally differ from the basic expectation. This is the case for a preheated ICM, with $L \propto M^{11/6}$, invoked by Evrard & Henry (1991) to reproduce the X-ray luminosity function in an $\Omega_m = 1$ cold dark matter cosmology. Observations of the $L-T$ relation find a steeper slope, $L \propto T^3$, than expected from self-similarity (Mushotzky & Scharf 1997; Fairley et al. 2000; Novicki et al. 2002). Models incorporating angular momentum in halos have been able to reproduce the steeper relations (Del Popolo et al. 2005).

In general, deviations from spherical symmetry and differences in formation history and dynamical state will produce variations in $f_{\rm ICM}$ and $g(y)$ among halos of fixed mass, leading naturally to some distribution $p(L|M,z)$ of soft band luminosity L. We employ here a log-normal conditional likelihood, with fixed dispersion $\sigma_{\ln L}$, centered on a power-law scaling relation

$$L \;=\; L_{15,0}\; \rho_c^s(z)\; M^p. \tag{3}$$

It is important to note that this equation characterizes the log mean behavior of a mass-limited population. Surveys that are incomplete in mass may differ from this.

For a given choice of model parameters, cluster counts in flux and redshift are generated by convolving $p(L|M,z)$ with the halo mass function of Jenkins et al. (2001) and applying a mean fractional flux error correction. Comparing to REFLEX survey counts (Böhringer et al. 2004) determines most likely parameters. Since the REFLEX survey is relatively shallow, we choose not to solve for general redshift evolution. Instead, we simply compare cases of self-similar ($s = 7/6$) and no ($s = 0$) evolution. For soft X-ray luminosities, the expected mass and redshift scalings are somewhat weaker than the bolometric case of equation (1), $L \propto M \rho_c(z)$, but we employ $s = 7/6$ as a slightly extreme variant.

Our analysis is therefore focused on the slope p, present-epoch intercept, $L_{15,0}$, at $10^{15}\,h^{-1}\,{\rm M}_\odot$, and the dispersion $\sigma_{\ln L}$, which we express in terms of the equivalent dispersion in mass $\sigma_{\ln M} = \sigma_{\ln L}/p$.

A more direct approach to the problem of relating luminosity to mass involves using individual cluster mass estimates derived under the assumption of strict hydrostatic and/or virial equilibrium. Reiprich & Böhringer (2002) (hereafter RB02) perform this analysis with 63 clusters from the flux-limited HIFLUGCS survey, finding consistency with the power-law expectation, equation (3), with a slope slightly steeper than self-similar and with a few tens of percent intrinsic scatter in mass at fixed luminosity. A promising future approach to this problem is to use weak lensing mass estimates of stacked cluster samples (Johnston 2005).

In §2, we explain the model and our approach to analyzing the REFLEX survey counts. In §3, parameter constraints that result from matching the counts are presented and found to be strongly degenerate. We therefore apply a pair of additional constraints, one based on the clustering of REFLEX clusters and the other on the observed scatter in the temperature-luminosity relation. The latter exercise requires input from cosmological simulations of clusters.

We compare to results of RB02 and discuss implications for cluster selection and hydrostatic mass estimates in §4. A summary and conclusions are given in §5. Except in §4, our calculations assume a concordance ΛCDM cosmology with $\Omega_m = 0.3$, $\Omega_\Lambda = 0.7$, $H_0 = 100h\,{\rm km\,s^{-1}\,Mpc^{-1}}$, and $\sigma_8 = 0.9$.

Throughout the paper, L is the X-ray luminosity in the rest-frame, soft ROSAT passband $(0.1 - 2.4~{\rm keV})$ in units of 10^{44} erg s^{-1} assuming $h = 0.7$. The mass M is taken to be M_{200}, the mass contained within a sphere whose mean interior density is $200\rho_c(z)$, expressed in units of $10^{15}\,h^{-1}\,{\rm M}_\odot$. The reader is hereby notified that we employ different Hubble constant conventions when presenting values for luminosity and mass.

2. MODELING THE LUMINOSITY FUNCTION

After briefly introducing the REFLEX cluster sample used in the analysis, this section details our approach to modeling cluster counts in flux and redshift, including evolutionary corrections.

2.1. *The REFLEX Survey*

We use cluster counts from the REFLEX (ROSAT-ESO-Flux-Limited-X-ray) Cluster Survey, which covers an area of 4.24 str and includes 447 identified galaxy clusters down to a flux limit of 3×10^{-12} ergs s^{-1} cm^{-2} in the (0.1 to 2.4 keV) ROSAT band (Böhringer et al. 2004). The X-ray clusters have been correlated with optical data from the COSMOS data base with a relatively low threshold to define a highly complete cluster candidate catalogue. Cluster validation and redshift determinations were achieved by an intense spectroscopic follow-up observing program at the European Southern Observatory, supplemented by available literature.

Luminosity determinations and the first REFLEX sample release are described in Böhringer et al. (2001). Determination of the survey selection function is described in Böhringer et al. (2002) and references therein. We do not incorporate selection function uncertainties directly into our analysis. This simplification is unlikely to significantly affect our conclusions, since at the high flux-limit of the REFLEX survey the sample is well understood. Böhringer et al. (2001) estimate a loss under 5% of clusters in low exposure regions, and tests presented in that work (*cf.*, Figure 25) show that this changes the derived luminosity function by less than 2%.

The redshifts and luminosities of the REFLEX clusters are shown in Figure 1. The solid lines are lines of constant flux: 4, 10, and 25×10^{-12} ergs s^{-1} cm^{-2} in the [0.1-2.4 keV] band. In the following section, we perform a likelihood analysis on this count distribution in flux and redshift.
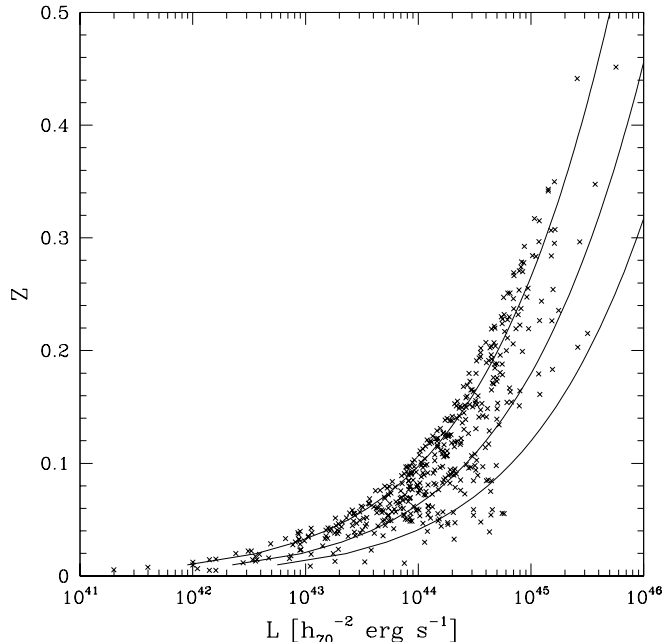
FIG. 1.— Redshifts and observed luminosities of 447 clusters in the full REFLEX survey. The solid lines are lines of constant flux: 4, 10, and 25×10^{-12} ergs s^{-1} cm^{-2} in the observed (0.1 to 2.4 keV) ROSAT band.

We must account for several survey effects when computing model expectations. Our basic model predicts the total flux while the REFLEX data are based on flux detected within the fixed angular aperture. We correct the data for this aperture effect by using the extrapolated fluxes calculated by Böhringer et al. (2001). This correction results in an 8% average increase in luminosity, but for a few bright nearby clusters the correction is larger.

We also include a K-correction in our model. The luminosity L in our mass-luminosity relation is the emissivity integrated over the rest-frame, 0.1-2.4 keV band, whereas the REFLEX data are derived from the emissivity over a band redshifted by a factor $(1 + z)$. We find that the K-correction used for the REFLEX survey construction, listed in Table 3 of (Böhringer et al. 2004), is well fit by the form

$$K(z,T) = \left(1 + (1 + \log_{10}[T/5\,\mathrm{keV}]\, z)\right)^{1/2} \tag{4}$$

where $L_{\mathrm{obs}} = K(z,T)\, L_{\mathrm{rest}}$. We assign temperatures to halos in a manner described below.

2.2. Theoretical Model

The space density of dark matter halos is now accurately calibrated for the case of hierarchical clustering from an initially Gaussian random density field. We use parameters derived for the mass scale M_{200} by Evrard et al. (2002), based on the Jenkins mass function (hereafter JMF, Jenkins et al. (2001)) form determined from a suite of cosmological simulations.

The JMF is described by a similarity variable $\sigma(M, z)$, where σ^2 is the variance in the linear density field after top-hat filtering fluctuations on mass scale M. The function $\sigma(M, z)$ is a monotonic decreasing function of mass for bottom-up models of structure formation and its inverse is well fit in the log by a quadratic relation, $\ln \sigma^{-1}(M, 0) = s_0 + s_1 \ln M + s_2 (\ln M)^2$. Fit parameters for specific models we employ are listed in Table 1. Jenkins et al. (2001) show that the mass fraction in halos of mass M at redshift z

$$f(M) \equiv \frac{M}{\rho_m(z)} \frac{\mathrm{d}n(M,z)}{d\ln\sigma^{-1}}, \tag{5}$$

is well fit by

$$f(M) = A\, \exp(-|\ln \sigma^{-1} + B|^\epsilon). \tag{6}$$

When evaluating the mass function, we use the fact that $\sigma(M, z)$ scales with the linear growth factor of density fluctuations $D(z)$. In addition, the parameters A, B vary linearly with Ω_m as described in Evrard et al. (2002). The $z=0$ values are listed in Table 1.

In a small comoving volume element dV at redshift z, we write the probability dp of finding a cluster of mass M and luminosity L as

$$dp = p(L|M,z)\, n(M,z) d\ln M d\ln L\, dV \tag{7}$$

We assume a log-normal conditional probability

$$p(L|M,z) = \frac{1}{\sqrt{2\pi}\sigma_{\ln L}} \exp\left[-\frac{(\ln L - \overline{\ln L})^2}{2\sigma_{\ln L}^2}\right] \tag{8}$$

with constant dispersion $\sigma_{\ln L}$ and a log-mean (or median) luminosity that follows

$$\overline{\ln L}(M, z) = \ln L_{15}(z) + p \ln M \qquad (9)$$

where the normalization

$$\ln L_{15}(z) = \ln L_{15,0} + s \ln \left[\rho_c(z)/\rho_c(0) \right] \qquad (10)$$

sets the luminosity of a cluster with mass $10^{15} h^{-1} M_\odot$ at redshift z.

In principle, the dispersion $\sigma_{\ln L}$ could be variable in mass or redshift, but we assume it to be constant, at least over the range of masses ($\gtrsim 3 \times 10^{13} h^{-1}$ M$_\odot$) and redshifts ($z \lesssim 0.3$) probed by the REFLEX sample. The same is true for the slope parameter p.

The luminosity function at any epoch is the conditional probability convolved with the JMF

$$dn(L, z) = \int d\ln M \; n(M, z) \, p(L|M, z) \, d\ln L. \qquad (11)$$

The number counts of clusters at redshift z with observed flux greater than f is

$$\frac{dN(>f, z)}{dz} = \frac{dV}{dz} \int_{L_{\min}(z)}^{\infty} dn(L, z) \qquad (12)$$

where $L_{\min}(z) = 4\pi d_L^2(z) f / K(z, T)$, with $d_L(z)$ the luminosity distance and $K(z, T)$ the K-correction fit of equation (4). We use the analytic luminosity distance approximation presented in Pen (1999). To calculate halo temperatures, we use the relation of Evrard et al. (2002) that reproduces the local temperature function in a concordance model

$$kT = 6.5 \, (h(z)M)^{2/3} \, \sigma_8^{-5/3} \, \text{keV}, \qquad (13)$$

with $h(z) = h(0)\left(\rho_c(z)/\rho_c(0)\right)^{1/2}$ the Hubble parameter at redshift z. For our choice of normalization, the $z=0$ intercept at $10^{15} h^{-1}$ M$_\odot$ is 7.7 keV.

With the log-normal assumption, equation (8), the flux-limited counts simply weight the mass function with a complementary error function giving the fraction of halos that satisfy the flux limit at each redshift

$$\frac{dN(>f, z)}{dz} = \frac{1}{2} \frac{dV}{dz} \int d\ln M \; n(M, z) \, \text{erfc} \left(y_{\min}(M, z) \right). \qquad (14)$$

with $y_{\min}(M, z) = [\ln L_{\min}(z) - \overline{\ln L}(M, z)]/\sqrt{2}\sigma_{\ln L}$.

Our likelihood analysis is based on differential counts in flux and redshift

$$\frac{d^2 N(f, z)}{dz \, d\ln f} = \frac{dV}{dz} \int d\ln M \; n(M, z) \, p(L|M, z) \qquad (15)$$

with $L = 4\pi d_L^2(z) f / K(z, T)$.

2.3. *Flux Errors*

We must incorporate flux uncertainties in the REFLEX survey into our analysis. The mean fractional error in cluster flux is not large, $\langle \delta f/f \rangle = 0.17$, but the individual errors tend to increase at lower flux levels. Approximating the flux errors as constant, we modify the theoretical predictions by convolving the raw predicted counts with a Gaussian in $\ln f$ of fixed width $\sigma = 0.17$. This fractional scatter adds in quadrature to the intrinsic model scatter.

To avoid clusters with flux errors substantially larger than the mean, we use a flux limit 4×10^{-12} erg s^{-1} cm^{-2} in the likelihood analysis, a few flux error sigma higher than the formal REFLEX flux limit 3×10^{-12} erg s^{-1} cm^{-2}. This reduces the sample size to 299 clusters but, because of the strong influence of the scatter constraint discussed in §3.3 below, the uncertainties in our final parameter estimates are not strongly affected by the reduced counts.

As a check on this approach to incorporating flux errors, we have used an alternative that compares the uncorrected theoretical counts to a Monte Carlo ensemble of REFLEX realizations created using the set of measured flux errors. The mean likelihood of the ensemble, using flux limit 4×10^{-12} erg s^{-1} cm^{-2}, produces parameter constraints that lie within 1σ of the results obtained using the convolution approach. We present our results using the latter method.

TABLE 1
FILTERED POWER SPECTRUM AND JMF PARAMETERS

Ω_m	s_0	s_1	s_2	A	B	ϵ
0.24	0.468	0.267	0.0123	0.216	0.737	3.86
0.30	0.549	0.281	0.0123	0.220	0.730	3.86
0.36	0.608	0.287	0.0123	0.224	0.723	3.86

2.4. *Redshift Evolution*

Ideally, we would include the evolution parameter s of equation (1) as a free parameter, along with $L_{15,0}$, p and $\sigma_{\ln M}$, in our analysis. But because of the relatively shallow sample, and the lack of uniform luminosity and redshift coverage (see Figure 1), we defer this exercise to future, deeper samples.

Instead, we limit our investigation to two distinct, and likely extreme, cases: the self-similar (SS) model of eq'n (1) and a no evolution (NE) model with $L_{15}(z) = L_{15,0}$. Self-similar evolution is supported by recent work of Maughan et al. (2005), who investigate the redshift behavior of the luminosity–temperature relation in a sample of eleven clusters to redshift $z \sim 1$. However, Ettori et al. (2004) do not see strong evolution to $z = 1.3$ in the luminosity–mass relation with a sample of 28 clusters.

2.5. *Parameter Degeneracies*

The convolution of the mass function is affected slightly differently by the three model parameters. An increase in $L_{15,0}$ simply shifts the luminosity scale to brighter values while the slope p controls the local slope of the luminosity function, with lower p being steeper. Changing $\sigma_{\ln M}$ produces a combination of the above effects, affecting both the shape and normalization. Over a finite range of luminosity, changes induced by varying one parameter can thus be offset by appropriate variations of the other two. One therefore anticipates degeneracies among the model parameters when fitting to counts alone.

For the case of a pure power law mass function $n(M) \propto M^{-\gamma}$, we show in the Appendix that the degeneracy is exact and takes the form

$$C \;=\; \ln L_{15,0} + (\gamma p/2)\sigma_{\ln M}{}^2, \tag{16}$$

where C is the quantity that is constrained by the data.

3. RESULTS

After first presenting parameter constraints that result from matching the REFLEX survey flux-limited counts, we extend the analysis to include clustering bias and scatter in the luminosity-temperature relation. We then compare our model results to those of RB02, and discuss the important role of flux-limited selection.

3.1. *Constraints from REFLEX counts*

We calculate likelihoods based on the expected survey counts in narrow flux and redshift bins, following the Poisson approach described in Pierpaoli et al. (2001). We define confidence intervals relative to the best fit model using $\ln\left(\frac{\mathcal{L}}{\mathcal{L}_{\max}}\right) = -\chi^2/2$, where $\mathcal{L}_{\max}$ is the maximum likelihood of all the models examined.

Figure 2 shows 68 and 99% confidence contours for the model parameters that result from matching the REFLEX survey counts. Each panel shows likelihoods marginalized over the missing parameter. Solid lines assume self-similar evolution of the luminosity while dashed lines assume no redshift evolution. Due to the degeneracy between the three parameters discussed in section 2.5, the observed counts are reproduced at 99% confidence over a fairly broad swath of parameter space. For the SS case, the slope can take values $1.55 < p < 1.85$, intercepts lie in the range $1.25 < L_{15,0} < 1.85$, and the scatter is bounded by $\sigma_{\ln M} < 0.42$. Zero scatter in the mass-luminosity relation, a seemingly unphysical solution given that cluster-sized halos are frequently dynamically active, is actually the most likely model, with slope $p = 1.70$ and $\ln L_{15,0} = 1.70$.

The NE model is shifted to a brighter intercept and steeper slope. The brighter intercept is needed to produce sufficient numbers of high luminosity clusters at moderate redshifts, while the steeper slope avoids overproducing counts at low luminosities and redshifts.

Figure 3 shows that the best fit SS and NE models provide good matches to the observed REFLEX counts in flux and redshift. Also plotted are discrete counts derived from the Hubble Volume (HV) mock sky catalogs (Evrard et al. 2002). For each halo, we assign a luminosity using parameters of the best-fit SS model, along with a temperature using equation (13). The K-corrected flux is then calculated and used to determine counts in mock surveys with REFLEX angular sky coverage. The lines in Figure 3 result from different random assignment of luminosities to halos using the best fit final parameter discussed in § 3.4.

To improve these parameter constraints we must include additional information from related observations or from theoretical priors derived, for example, from numerical simulations. We follow a largely empirical approach, and move on in the following sections to add constraints from the effective bias of the REFLEX survey and from the scatter in the observed temperature–luminosity relation. As explained below, interpreting the T-L scatter requires input from cosmological simulations.

3.2. *Clustering Bias*

Massive halos display stronger spatial clustering than the density field in general (Kaiser 1984). The halo–halo power spectrum $P_{\rm hh}(k)$ for mass-limited samples exhibits a nearly constant, mass-dependent bias $b(M) = \sqrt{P_{\rm hh}/P}$ on large scales. We use the form for this bias derived by Sheth & Tormen (1999),

$$b(M) = 1 + \frac{1}{\delta_c}\left[\frac{a_s\delta_c^2}{\sigma^2} - 1 + \frac{2p_s}{1 + (a_s\delta_c^2/\sigma^2)^{p_s}}\right] \tag{17}$$
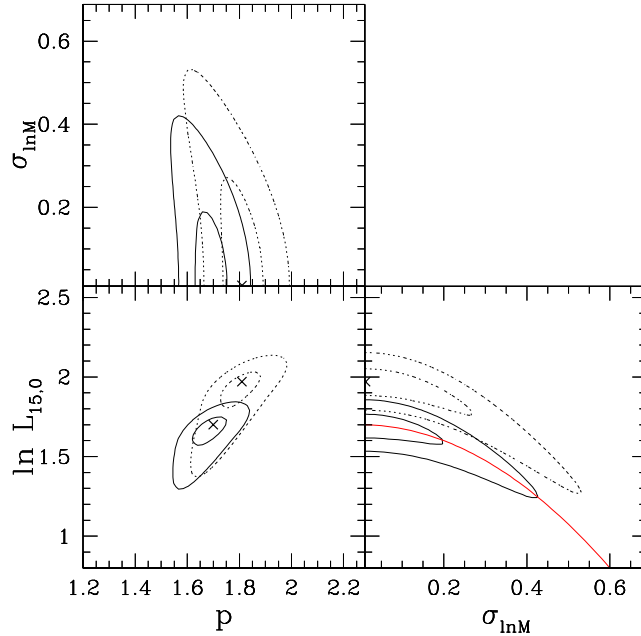
FIG. 2.— Contours of the 68 and 99% marginalized likelihoods of the model parameters that result from matching the REFLEX counts are plotted for self-similar (solid) and no evolution (dashed) assumptions. Crosses mark the maximum likelihood of the three-parameter model. The added curve in the lower right-hand panel plots the degeneracy between $\sigma_{\ln M}$ and $\ln L_{15,0}$ expected for a power-law number function, equation (16).
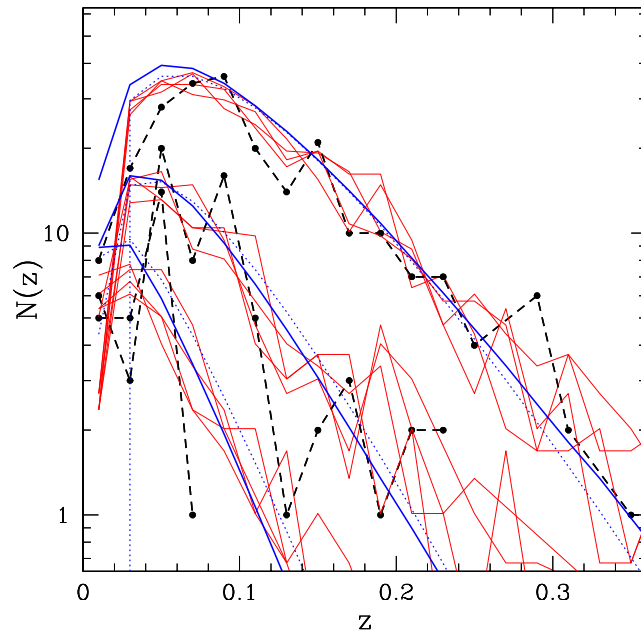

FIG. 3.— Differential counts in redshift for three flux ranges (from upper to lower): $4 \leq f < 10$, $10 \leq f < 25$, and $f \geq 25 \times 10^{-12}$ erg s^{-1} cm^{-2}. The REFLEX data are plotted as filled circles, while the counts expected from the best-fit SS (solid) and NE (dotted) models are shown as continuous lines. Light solid lines for each flux range show discrete realizations using discrete mock sky catalogs and the best-fit SS model.

with parameter values $\delta_c = 1.68$, $a_s = 0.75$ and $p_s = 0.3$ from Hu & Kravtsov (2003a). The effective bias of a volume-limited sample centered at (low) redshift z is then

$$b_{eff} = \frac{\int d\ln M \, w(M,z) \, n(M,z) \, b(M)}{\int d\ln M \, w(M,z) \, n(M,z)} \tag{18}$$

where $w(M,z)$ is a weight function that gives the fraction of halos of mass M that lie above the minimum luminosity L_{min} of the sample at redshift z. We calculate the bias appropriate for the volume-limited sample L050 in Schuecker
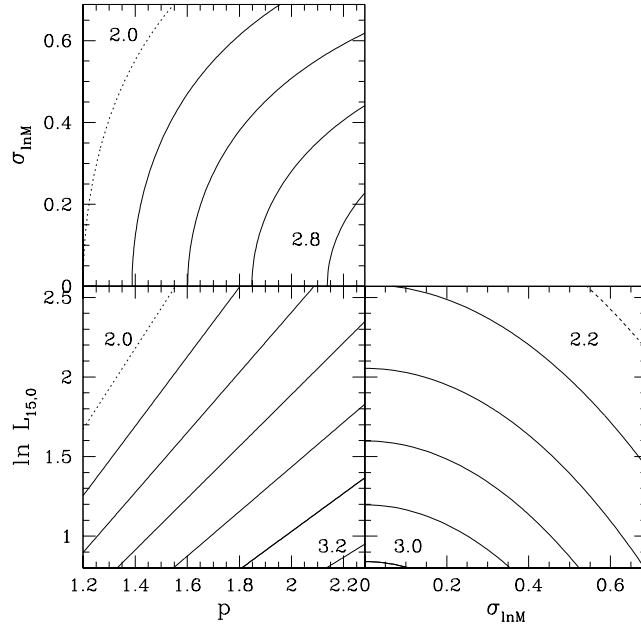
FIG. 4.— Contours of the effective bias b_{eff} are shown in slices through parameter space at the SS best-fit location of Fig 2. Contours are spaced by 0.2.

et al. (2001), with $L_{min} = 2.55 \times 10^{43} h_{70}^{-2} erg\ s^{-1}$ and mean redshift $z = 0.04$. We do not take into account any redshift dependence of the bias, which will be small for this sample.

Figure 4 plots contours of b_{eff} for slices within the model parameter space centered on the best-fit location of the SS model in Figure 2. As p increases, the range of halo masses sampled decreases, implying a higher minimum mass scale and therefore an increasing bias. The effective bias decreases as $\ln L_{15,0}$ increases due to the fact that lower mass halos satisfy the flux limit. Finally, increasing $\sigma_{\ln M}$ causes a decline in the effective bias, because increased scatter adds lower-mass halos at a fixed luminosity.

The power spectrum and uncertainties published for this sample by Schuecker et al. (2001) imply a prior on the effective bias of $b_{eff} = 3.0 \pm 1.0$ for a concordance cosmology. As shown in Figure 4, the 1σ uncertainty on the effective bias nearly fills the parameter space we are considering. Because of the large uncertainty, adding the bias constraint does not significantly improve the fits from counts alone. More precise measurement of the clustering bias will require deeper surveys that better probe the high mass/high bias portion of mass function.

3.3. *Scatter in the Luminosity-Temperature Relation*

We next derive information on the mass variance $\sigma_{\ln M}^2$ from the intrinsic scatter of the temperature–luminosity relation. Figure 5 shows the T-L relation for 106 HIFLUGCS clusters published by RB02, with temperatures obtained from various original sources. We fit the relation to a power law, including the stated errors in temperature, and then measure the intrinsic variance $\sigma_{\ln T|L}^2$ by subtracting the measurement error contribution from the total variance. We bootstrap over the quoted errors on the temperatures to estimate the uncertainty in the intrinsic dispersion, with the result $\sigma_{\ln T|L} = 0.25 \pm 0.03$. While there are other cluster surveys with luminosity and temperature data (Horner 2001; Ikebe et al. 2002), we use temperatures from RB02, to be consistent throughtout the paper.

To include the measured T-L scatter in the analysis, consider a mass-limited ensemble of co-eval halos with masses, X-ray spectral temperatures and soft X-ray luminosities $\{M_i, T_i, L_i\}$. Motivated by the virial theorem, and mirroring the case for luminosity, we assume that T and M are related by a power-law with log-normal scatter, and write $\overline{\ln T} = \ln T_{15} + q \ln M$. Any given halo will, in general, deviate from the mean L-M and T-M scalings. The ith cluster's true mass $\ln M$ will deviate from the values inferred by inverting the log-mean relations for its temperature and luminosity

$$\ln M = \frac{1}{q} \ln \left(\frac{T}{T_{15}} \right) + \delta_T^M, \tag{19}$$

$$\ln M = \frac{1}{p} \ln \left(\frac{L}{L_{15}} \right) + \delta_L^M. \tag{20}$$

The halos temperature and luminosity are then related by

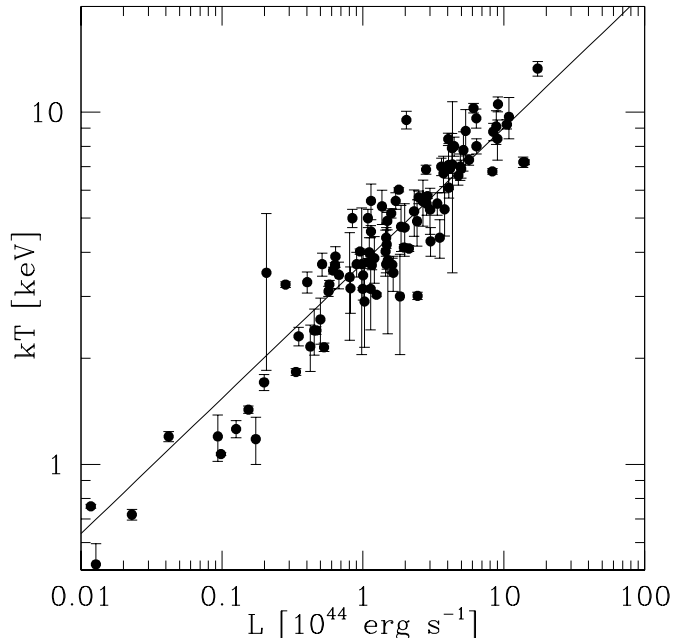$$\ln T = \frac{q}{p} \ln L + \ln T_{15} - \frac{q}{p} \ln L_{15} + q(\delta_L^M - \delta_T^M), \tag{21}$$

FIG. 5.— The T-L relation for HIFLUGCS clusters from Reiprich & Böhringer (2002). Error bars indicate the observed 1σ uncertainties in the temperature measurements.

so, considering a subset of halos of fixed luminosity L, the expected T-L relation is

$$\langle \ln T \rangle \;=\; \frac{q}{p}\,\ln L + C, \tag{22}$$

where $\langle\,\rangle$ represents an average at fixed luminosity. The intercept $C = \ln T_{15} - \frac{q}{p}\ln L_{15} + q[\langle \delta_L^M \rangle - \langle \delta_T^M \rangle]$ will be biased from the zero-scatter expectation if the mean mass deviations based on temperature and luminosity do not cancel, $\langle \delta_T^M \rangle \neq \langle \delta_L^M \rangle$.

The second moment $\langle (\ln T - \langle \ln T \rangle)^2 \rangle$ of the observed T-L relation yields

$$\sigma_{\ln T|L}^2 = q^2 \big[\langle (\hat{\delta}_L^M)^2 \rangle - 2\langle \hat{\delta}_L^M\,\hat{\delta}_T^M \rangle + \langle (\hat{\delta}_T^M)^2 \rangle \big], \tag{23}$$

where $\hat{\delta}_L^M \equiv \delta_L^M - \langle \delta_L^M \rangle$ and $\hat{\delta}_T^M \equiv \delta_T^M - \langle \delta_T^M \rangle$ are deviations from the sample means, again at fixed luminosity.

We show below that flux-limited samples are biased in favor of low-mass halos $\langle \delta_L^M \rangle < 0$, but we also find that the measured mass variance in mock HIFLUGCS samples is nearly unbiased relative to a complete, mass-limited sample. We therefore assume $\sigma_{\ln M|L}^2 = \langle \hat{\delta}_L^{M\,2} \rangle$. Noting that the variance of our underlying model is $\sigma_{\ln M}^2 = \sigma_{\ln M|L}^2$, then equation (23) can be rearranged to give

$$\sigma_{\ln M}^2 = \frac{\sigma_{\ln T|L}^2}{q^2} - \sigma_{\ln M|T}^2 + 2\langle \delta_L^M\,\delta_T^M \rangle. \tag{24}$$

This equation links the variance in mass at fixed luminosity to an observable quantity, the T-L variance $\sigma_{\ln T|L}^2$, along with other terms that are not directly observable. To evaluate these terms, we turn to an ensemble of 68 cluster simulations evolved under a 'preheated' assumption (Bialek & Evrard 2006). Like previous simulations (Evrard et al. 1996; Bryan & Norman 1998; Mathiesen & Evrard 2001a; Borgani et al. 2004; Rasia et al. 2004), these models respect the virial scaling between temperature and mass, displaying a logarithmic mean relation $T \propto M^{0.58 \pm 0.02}$ that is slightly shallower in slope than the self-similar value of 2/3 due to the enhanced effects of the raised initial entropy on low mass systems. To approximate actual temperature estimates, the temperature T is determined from fitting mock X-ray spectra of each simulated cluster, assuming emission from a plasma enriched to 0.3 solar metallicity.

Figure 6 shows the frequency distribution of the residuals in mass estimates based on inverting the mean virial relation for the 68 clusters sampled at six low-redshift epochs, $z = 0.290, 0.222, 0.160, 0.102, 0.49$ and 0. The distribution of logarithmic deviations is very close to Gaussian, with dispersion $\sigma_{\ln M|T} = 0.19$. This small scatter is empirically supported by the work of Mohr et al. (1999), who find $\sim 17\%$ scatter in M_{ICM} at fixed temperature.

We use data from the same models to examine the covariance in the M-L and M–T deviations, shown in Figure 7. The simulations display weak covariance $\langle \delta_T^M\,\delta_L^M \rangle = 0.017$. The weak coupling presumably arises because T and L are sensitive to processes operating on different scales and because the effects of multiple mergers, rather than a single dominant encounter, are driving the halo dynamics at most times. This finding may seem at odds with results from binary merger simulations by Ricker & Sarazin (2001). In the binary case, the luminosity and temperature rise and fall in concert as the mass increases during the merger, suggesting strong covariance. However, recent cosmological simulations
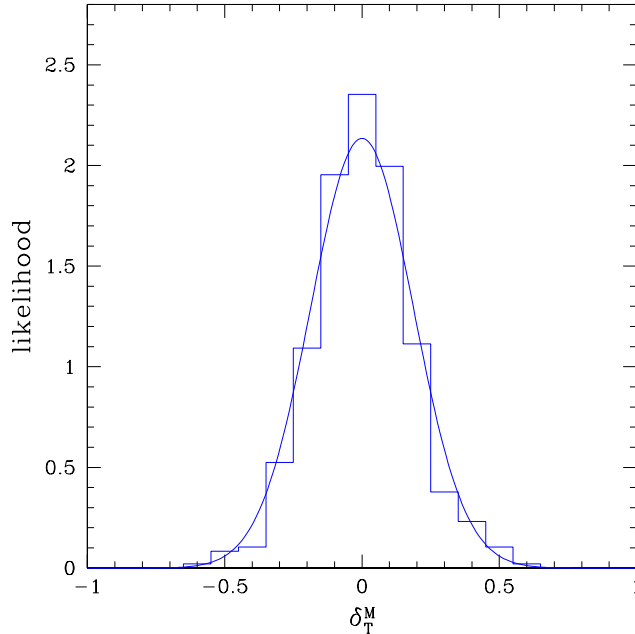
FIG. 6.— The histogram shows deviations in (natural) log mass from mean power-law fits to the $M - T$ relation from 68 preheated cluster simulations (Bialek & Evrard 2006). The solid line shows a Gaussian fit with zero mean and dispersion of 0.19
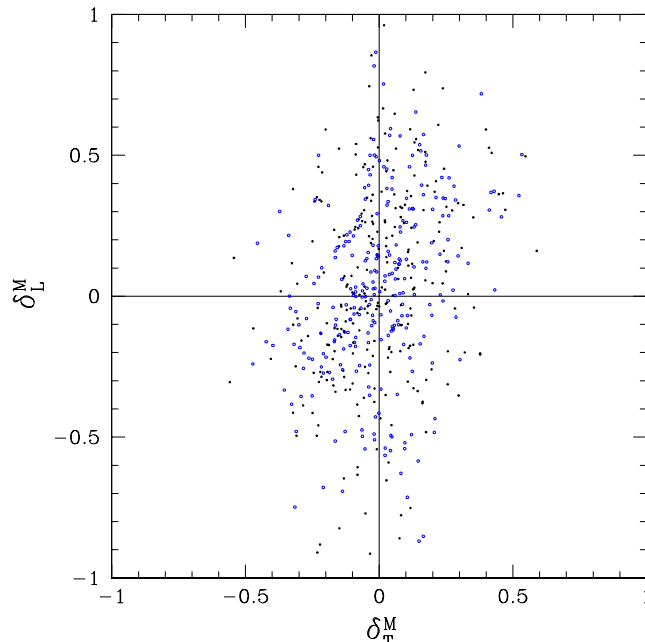

FIG. 7.— The correlation of residuals in log mass about the mean M-T and M-L relations derived from 68 preheated cluster simulations (Bialek & Evrard 2006) at epochs $0 < z < 0.2$ (filled circles) and $0.2 < z < 0.3$ (open circles).

by Rowley et al. (2004) show complex evolution in L and T during cluster evolution that is more aligned with the results of Figure 7.

With these estimates in hand, and with $\sigma_{\ln T|L}$ from the RB02 data, we find the scatter in mass at fixed luminosity from equation (24) to be

$$\sigma_{\ln M} = 0.43 \pm 0.06, \tag{25}$$

where we have assumed a T-M slope $q = 0.58 \pm 0.05$, equivalent to $M \propto T^{1.72 \pm 0.12}$. The slope uncertainty, along with the intrinsic T-L scatter measurement error, dominate the uncertainty in $\sigma_{\ln M}$. Note that a self-similar T-M scaling, $q = 2/3$, leads to a 1σ reduction in scatter, $\sigma_{\ln M} = 0.37$.
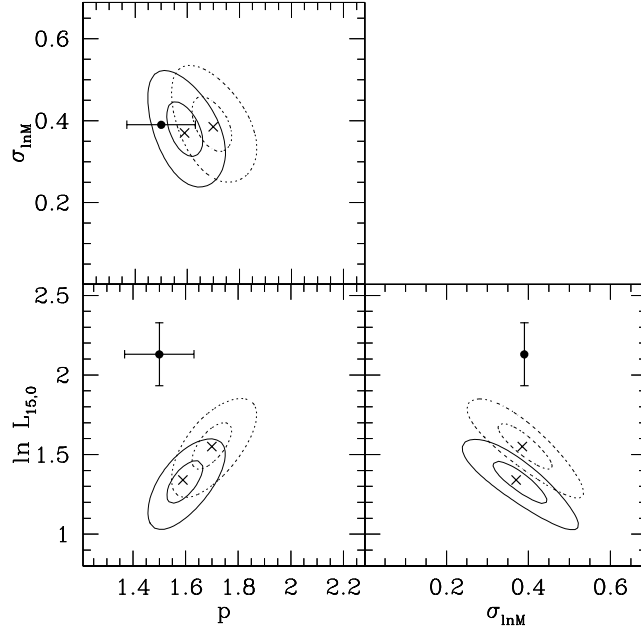
3.4. Full Constraint Results

FIG. 8.— Marginalized 68 and 99% confidence intervals are shown after including constraints from clustering bias and from the estimated scatter of equation (24). Solid and dotted lines are SS and NE models. Crosses mark the maximum likelihood location. The data point is the RB02 result, shown with 90% confidence error bars on the slope and intercept.
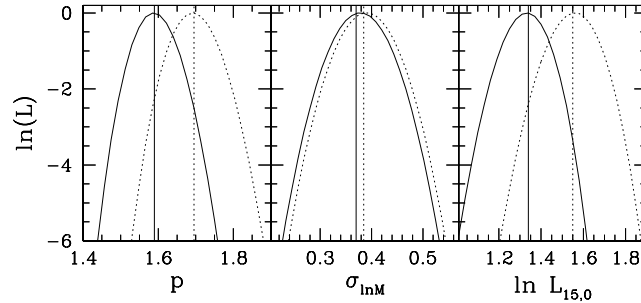

FIG. 9.— One-dimensional, marginalized likelihoods for each model parameter for the SS (solid) and NE (dotted) models after applying the constraints used in Figure 8. Vertical lines denote the maximum likelihood location in the full parameter space.

Adding the constraint of equation (25), along with the effective bias, to the analysis produces the marginalized likelihoods plotted in Figures 8 and 9. This analysis yields values $p = 1.59 \pm 0.05$, $\ln L_{15,0} = 1.34 \pm 0.09$, and $\sigma_{\ln M} = 0.37 \pm 0.05$. These values are strongly dependent on the scatter constraint, and thus depend on the measurements of temperature, luminosity, and their quoted errors, all of which determine $\sigma_{\ln T|L}$.

The solid circle in Figure 8 shows parameter values from RB02. Because the published values assumed $\Omega_m = 1$, we have made small (typically few percent) corrections to convert their luminosity and mass estimates to a concordance cosmology. Under an isothermal profile assumption ($\rho(r) \propto r^{-2}$) used by RB02, the correction to cluster mass scales as $\rho_c^{-1/2}(z)$, while the luminosity scales as $d_L^2(z)$, with d_L the luminosity distance.

Fitting corrected luminosity to mass, we find best-fit values $p = 1.50 \pm 0.08$ and $\ln L_{15,0} = 2.13 \pm 0.12$ for the slope and intercept of the RB02 sample. Subtracting in quadrature the measured mass uncertainties from the scatter in the L-M relation, we find an estimate of the intrinsic scatter, $\sigma_{\ln M} = 0.39$. A formal uncertainty in this estimate is complicated by the fact that there are several sources of scatter, including variance in the hydrostatic mass estimator, that are not easily separated. We defer this exercise to future work. The fact that this estimate of the intrinsic M-L scatter agrees with our model results suggests that the scatter in hydrostatic mass estimates is less than $\sigma_{\ln M}$.

The RB02 normalization result is in serious conflict with the value determined here. We address the main source of this discrepancy, and discuss other implications, in the following section.

Note that the slope, q/p, inferred for the T-L relation via equation (22) is 0.36 ± 0.03, in reasonable agreement with the $T \sim L^{0.45 \pm 0.04}$ displayed by the data in Figure 5. A self-similar slope, $q = 2/3$, yields better agreement, $q/p = 0.42$, but the data do not compel this choice.
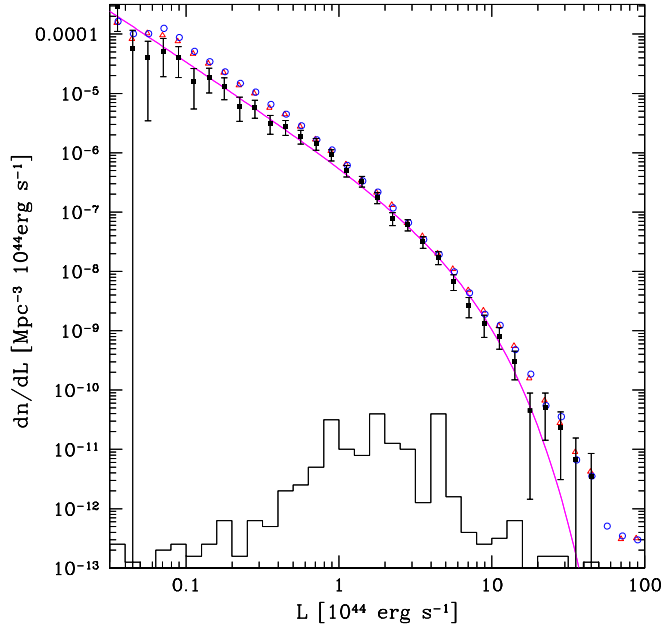
FIG. 10.— The luminosity function of the REFLEX data (filled squares), shown with 1σ uncertainty from Poisson and flux errors, is compared to mock HV sample results using the best fit SS (open circles) and NE (open triangles) parameters from Figure 8. The solid line is the Schecter function fit to the luminosity function from Böhringer et al. (2001). The histogram shows raw REFLEX counts in 0.1 dex luminosity bin, using a linear scale of 10 counts per decade.

As a further comparison of the model and data, we show in Figure 10 a binned representation of the luminosity function of the REFLEX data, determined with a $1/V_{\max}$ sum described in Böhringer et al. (2001), along with discrete realizations of the function derived from HV mock sky catalogs using the best-fit SS and NE parameters (circles and triangles, respectively). Errors in the binned data include contributions from flux errors and Poisson fluctuations. At low luminosities, the sample variance due to the small volume probed becomes significant. The histogram shows raw REFLEX counts in 0.1 dex luminosity bins.

The mock realizations provide a good match to the REFLEX luminosity function above $\sim 4 \times 10^{43}$ erg s^{-1}, where the survey counts per bin exceed ten. At lower luminosities, the models predict higher space densities than those observed. The small numbers of clusters makes it difficult to assess the nature of these differences. It may signal a breakdown in our model, perhaps through a steepening of the slope p at low luminosities. Alternatively, the REFLEX survey may be slightly incomplete at the low luminosity end, which is populated mainly by nearby, extended systems near the survey flux limit. This interpretation is supported by the finding of a 'local void' within $z \lesssim 0.03$ in the cluster spatial distribution (Schuecker et al. 2001). At the bright end, both the observed and model counts decline more slowly than a pure Schechter form, $dn/dL \propto e^{-L/L_*}$.

4. DISCUSSION

In this section, we first discuss the source of the discrepancy between the M-L relations derived here and that of RB02. We then briefly explore sensitivity of the model parameters to cosmology, focusing on changes to σ_8 and Ω_m. We then comment on theoretical uncertainty in the mass function, discuss connections to previous REFLEX analysis, and finish with remarks on the accuracy of isothermal beta mass estimates.

4.1. Selection Bias from Flux Limit

The results presented in Figure 8 indicate that the independent estimate of the luminosity–mass relation from RB02, based on isothermal β-model binding mass estimates, disagrees with the best-fit L-M relation derived above. There is reasonable agreement in the slope and scatter, but the RB02 intercept is substantially brighter than the best-fit values of both the SS and NE model results.

The large discrepancy in $\ln L_{15,0}$ results largely from a classical Malmquist bias expected in flux limited samples such as HIFLUCGS. For a given mass and redshift, a portion of the tail of low-luminosity clusters is lost due to the application of the flux limit. The amplitude of the resultant bias depends on the scatter in the mass-luminosity relation. We first calculate the expected bias analytically, then demonstrate it using mock realizations of flux-limited samples.

With our model, the expected log mean luminosity ($y \equiv \ln L$) as a function of mass ($x \equiv \ln M$) for a flux-limited sample is

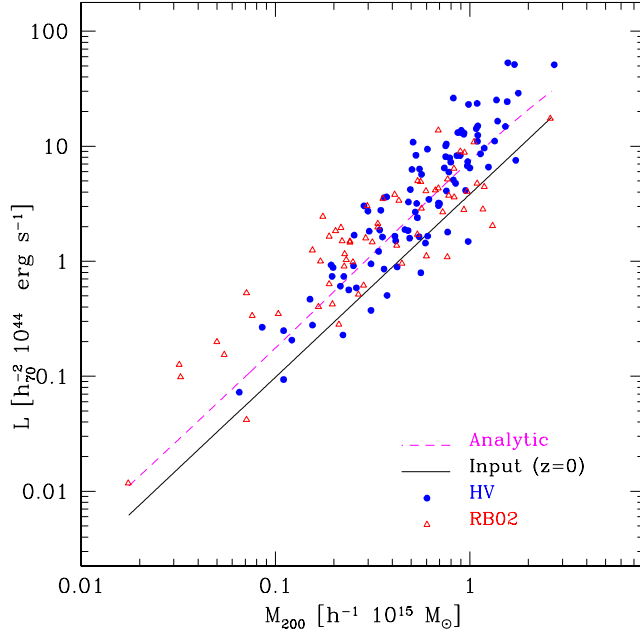$$\langle y(x) \rangle \quad = \frac{1}{dN_f(x)} \int dV(z)\, n(x,z)\, Y(x,z) \tag{26}$$

FIG. 11.— The best fit SS model relation between rest-frame, soft X-ray luminosity and mass at $z=0$ (solid line) is compared to the relation expected from a HIFLUCGS flux-limited sample (dashed line), computed from equation (27). Triangles show the HIFLUGCS data while filled circles show an HV mock version of these data.

$$Y(x,z) = \tfrac{1}{2}\bar{y}(x,z)\mathrm{erfc}(t_{\min}) + \sqrt{\tfrac{1}{2\pi}}\sigma_y e^{-t_{\min}^2} \qquad (27)$$

where $dV(z)$ is the comoving volume element at redshift z, $t_{\min} = (y_{\min} - \bar{y}(x,z))/\sqrt{2}\sigma_y$, $y_{\min} = \ln L_{\min}(x,z)$, $\bar{y}(x,z) = \overline{\ln L}(x,z)$, and $\sigma_y = \sigma_{\ln L} = p\,\sigma_{\ln M}$. As before, $L_{\min}(x,z) = 4\pi d_L^2(z)f/K(z,T)$ is the K-corrected minimum luminosity required to satisfy the flux limit at redshift z. The normalization $dN_f(x)$ is the differential number of halos of mass e^x that satifsy the flux limit

$$dN_f(x) \;=\; \frac{1}{2}\int dV(z)\,n(x,z)\,\mathrm{erfc}(t_{\min}). \qquad (28)$$

We employ this model, with the JMF assuming a concordance cosmology with our best-fit SS parameters, to calculate the L-M relation expected for the HIFLUGCS survey, with ROSAT soft-band flux limit $2\times10^{-11}\mathrm{ergs}^{-1}\mathrm{cm}^{-2}$. The result is shown as the dashed line in Figure 11. The HIFLUGCS sample systematically selects brighter objects at fixed mass, leading to a brightening, by roughly a factor two, in the L-M relation relative to the present epoch relation, shown as the solid line.

The brightening for this high flux sample results mostly from scatter, and not from evolution in the SS model. Figure 12 demonstrates this by comparing the increase, relative to $z=0$, in log mean luminosity, calculated from equation (27) for SS and NE models. At low masses and luminosities, the volume probed is small, and there is little evolution in the SS model. Above $10^{14}\,h^{-1}$ M$_\odot$, the survey depth is approaching $z\sim0.1$, and the SS model bias becomes larger than that of the NE model. As the survey probes to higher redshifts at higher masses, the SS model bias continues to grow up to $M\sim10^{15}\,h^{-1}$ M$_\odot$. Beyond this mass scale, the bias drops because the number of the most massive halos falls to zero at high redshift. A similar decline is seen in the NE model.

In addition to the analytic calculation, we also create mock realizations of the HIFLUGCS sample using HV sky survey samples. We assign a luminosity and temperature to each halo in a manner consistent with our best-fit model, and apply the flux cut to K-corrected fluxes. The result for one random realization is shown as filled circles in Figure 11. The points scatter about the analytic expectation with *rms* deviation of $\sigma_{\ln L}=0.63$, close to the input (mass-limited) scatter of 0.59. Due to the finite size of the HIFLUGCS sample, the degree of bias will vary from the analytic expectation. We estimate this variance using 200 Monte Carlo realizations of HV mock samples, derived from the MS and VS sky surveys (Evrard et al. 2002), adjusted to a sky area of 5.5 str to match the cluster counts in RB02. From this exercise, we derive correction terms of -0.70 ± 0.11 to $\ln L_{15,0}$ and -0.06 ± 0.07 to p. The correction terms strongly depend on the degree of scatter in the L-M relation.

4.2. Degeneracy and Cosmology

The normalization $\ln L_{15,0}$, amount of scatter $\sigma_{\ln M}$, and power spectrum normalization σ_8 are strongly coupled parameters that control the number counts. In the current approach, we determine the scatter via measurement of variance in the L-T relation, using input from simulations in a manner described in §3.3. The rather large scatter in luminosity
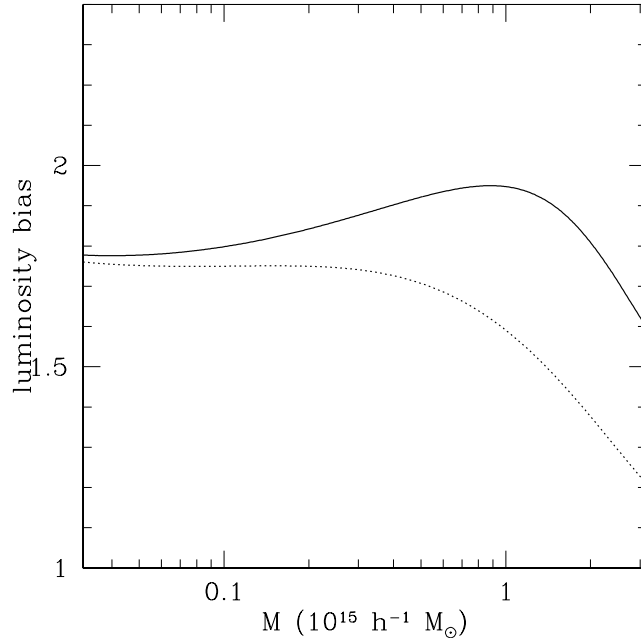
Fig. 12.— The ratio between the logarithmic mean luminosity of a 1.7×10^{-11} erg s^{-1}cm^{-2} flux-limited sample and the $z = 0$ relation is shown for the best-fit SS (solid) and NE (dotted) models. The difference in the two models is the result of redshift evolution, which is more important for higher mass halos that satisfy the sample flux limit at larger distances.

for halos of a given mass, $\sigma_{\ln L} = 0.59$, implies the signficant Malmquist bias discussed above. Previous analysis of the REFLEX cluster abundance and power spectrum (Schuecker et al. 2001, 2003) assumed a much smaller level scatter, $\sigma_{\ln L} \sim 0.2 - 0.3$, based on the impression that the main contribution to the L-M scatter derived in RB02 was large uncertainty in the binding mass measurement. With the smaller assumed scatter, no Malmquist bias correction was applied, so the value of $\ln L_{15,0}$ employed was higher, and the corresponding value of σ_8 lower, compared to the values used here. This approach has recently been emphasized by (Reiprich 2006).

The set of parameters allowed by Figure 8 assumes a concordance cosmological model described in § 1. We now explore the sensitivity of the best-fit location to changes in cosmological parameters (Ω_m, σ_8), under a flat-metric assumption. In particular, we focus below on the world model favored by year-three WMAP analysis (Spergel et al. 2006), which involves a lower normalization $\sigma_8 = 0.76 \pm 0.05$ and matter density $\Omega_m = 0.234 \pm 0.035$.

The left panel of Figure 13 shows how the results of our likelihood analysis change as the cosmology is varied. The dotted and dashed lines show 68 and 99% marginalized contours for $\Omega_m = 0.24$ and $\Omega_m = 0.36$, respectively. The power spectrum normalization is varied to keep $\sigma_8^2 \Omega_m$ constant, a condition that roughly holds fixed the number of halos above $\sim 2 \times 10^{14} h^{-1} M_\odot$ (Efstathiou, Frenk & White 1993; Viana & Lyddle 1998). The vacuum energy density $\Omega_\Lambda = 1 - \Omega_m$ is adjusted to maintain a flat metric. The shape of the filtered power spectrum $\sigma(M)$ is determined from CMBFAST (Seljak & Zaldarriaga 1996) and we use equation (11) of Evrard et al. (2002) to adjust the constants $A(\Omega_m)$ and $B(\Omega_m)$ in the JMF. Parameter values are listed in Table 1.

The constraint from the observed scatter in the T-L relation ties the best-fit location to a narrow range of $\sigma_{\ln M}$. However, as Ω_m increases, the slope of the mass function steepens, and the best fit value of p must increase as a result. We find that the slope scales roughly as $p \propto \Omega_m^{0.5}$, being reduced to $p = 1.46 \pm 0.04$ for $\Omega_m = 0.24$ and increased to 1.71 ± 0.05 for $\Omega_m = 0.36$ for the case of SS evolution. Table 2 lists the best fit SS parameters for these cosmologies.

For the most massive and X-ray luminous halos, a change of normalization σ_8 produces a nearly constant shift in the mass function in the mass direction, such that the mass M_* at fixed space density n_* scales as $M_* \propto \sigma_8^{1/\alpha'}$, with

TABLE 2
SS MODEL PARAMETERS FOR DIFFERENT COSMOLOGIES

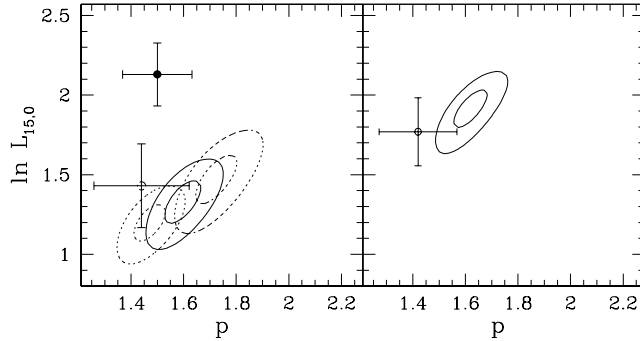| Ω_m	$\ln L_{15,0}$	p	$\sigma_{\ln M}$
0.24	1.19 ± 0.08	1.46 ± 0.04	0.39 ± 0.05
0.30	1.34 ± 0.09	1.59 ± 0.05	0.37 ± 0.05
0.36	1.46 ± 0.11	1.71 ± 0.05	0.37 ± 0.05

FIG. 13.— The left panel plots 68 and 99% confidence intervals of the slope and normalization for $\Omega_m = 0.24$, 0.3 and 0.36 (left to right), with $\Omega_m \sigma_8^2$ constant, after applying the joint constraints on counts, clustering, and $\sigma_{\ln M}$ scatter. The solid point in the left panel plots the original RB02 result, with 90% error bars. The right panel plots 68 and 99% confidence intervals of the slope and normalization for the WMAP compromise cosmology, $\Omega_m = 0.24$, $\sigma_8 = 0.85$, after applying the joint constraints on counts, clustering, and a lower $\sigma_{\ln M} = 0.25$ scatter. In both panels, the open point gives the RB02 result after correcting for the flux cut bias, with 90% error bars that include the variance of HV Monte Carlo realizations discussed in the text.

$\alpha' = 0.4$ above $\sim 2 \times 10^{14} h^{-1}$ M$_\odot$ (Evrard et al. 2002). Since observations fix the luminosity at n_*, variations in σ_8, and hence the mass scale M_*, can be compensated by adjusting the normalization $L_{15,0} \propto M_*^{-p}$. We therefore expect $L_{15,0} \propto \sigma_8^{-p/\alpha'}$. With $\alpha' \simeq 0.4$, and $p \simeq 1.6$, the characteristic luminosity should have strong sensitivity to the power spectrum normalization, $L_{15,0} \propto \sigma_8^{-4}$.

The open symbol in the left panel of Figure 13 shows the RB02 result, after correction for the flux bias described in the preceding section. Error bars have been enlarged by adding in quadrature the scatter in the corrections derived from the mock HV Monte Carlo analysis. The corrected results lie very close to the values determined here.

The right hand panel offers a compromise model driven by cosmological parameters from the WMAP Year 3 data (Spergel et al. 2006). The model assumes a flat metric with $\Omega_m = 0.24$ and a slightly elevated normalization $\sigma_8 = 0.85$, along with a reduced estimate of the scatter $\sigma_{\ln M} = 0.25 \pm 0.06$. The resulting best fit parameters are $p = 1.60 \pm 0.05$, $\sigma_{\ln M} = 0.21 \pm 0.06$, and $\ln L_{15,0} = 1.92 \pm 0.08$. The lower scatter leads to a smaller Malmquist bias for the RB02 sample, we derive corrections of -0.36 ± 0.05 to $\ln L_{15,0}$ and -0.08 ± 0.04 to p. The corrected RB02 result is then $p = 1.42 \pm 0.09$, $\ln L_{15,0} = 1.77 \pm 0.13$, and is plotted in the right-hand panel in Figure 13.

We concur with the analysis by Reiprich (2006) that a zero-scatter solution with $\sigma_8 = 0.76$ provides good agreement with the original RB02 result, but we feel that a zero-scatter solution is unphysical. The large variance in the observed T-L relation has been tied to variations in core emission (Fabian et al. 2006; O'Hara et al. 2006). Maintaining a tight L-M relation would require a strong coupling between core gas physics and total halo mass, as well as a large scatter in the virial (T-M) relation. These outcomes are neither anticipated theoretically nor supported by the current generation of numerical simulations.

4.3. Theoretical Uncertainty

Our model rests on the calibration of the M_{200} halo space density (Evrard et al. 2002). A full treatment of the theoretical error in the mass function is beyond the scope of this paper, but we comment here on the impact of normalization uncertainties in $n(M, z)$ on the $\ln L_{15,0}$ parameter.

Simulations by Hu & Kravtsov (2003b) find agreement with the form we employ at better than ten percent in number over the mass range $5 \times 10^{13} - 10^{15} h^{-1}$ M$_\odot$ (see their Fig. B10). The JMF calibration using percolation, rather than spherical overdensity, masses has been confirmed at the five percent level in number by Warren et al. (2005) using a set of sixteen 1024^3-particle simulations. That work proposes a slightly more complex formulation to replace our use of equation (6), but the difference at high masses is only a few percent in number (see their Fig. 2).

These results appear to indicate that the current calibration uncertainty in the halo space density is at the level of $\sim 5\%$ in number. For massive, X-ray luminous halos, where locally $d\ln n/d\ln M \simeq -3$, this translates into an error in mass scale of $\sim 2\%$, or an additional ~ 0.03 uncertainty in $\ln L_{15,0}$.

However, Warren et al. (2005) also find that one out of four non-concordance simulations shows a larger discrepancy

with the model expectations, roughly 20% in number. Considering that this is one outlier out of 20 simulations, and given that the remaining N-body data show much better consistency, we feel that a 15% uncertainty in number density is a conservative upper limit on the theoretical error. This implies a maximum additional uncertainty in $\ln L_{15,0}$ of ~ 0.08. The theoretical uncertainty is most likely smaller than, or, at worst, comparable to, the statistical error of 0.09.

The use of M_{500} as a mass measure is not expected to affect the theoretical uncertainties. Assuming an NFW mass profile, Appendix B of Evrard et al. (2002) calculates a simple shift to the mass scale. Shifting the mass scale results in a shift of the JMF, and our normalization parameter would likewise be translated.

4.4. *Accuracy of Hydrostatic Mass Estimates*

The isothermal β-model masses employed by RB02 are determined by fitting the azimuthally-averaged X-ray surface brightness to derive the gas density profile under the assumption of isothermality for the intracluster gas. Simulations indicate that this approach may yield masses that are biased by up to a few tens of percent (Evrard 1990; Schindler 1996; Navarro et al. 1995; Evrard et al. 1996; Rasia et al. 2004, 2006), but the computational expectations are rendered uncertain by incomplete modeling of ICM physics and by systematic errors associated with determining the spectral temperature derived from the thermally complex intracluster medium of simulated clusters (Mathiesen & Evrard 2001b; Mazzotta et al. 2003; Vikhlinin et al. 2005). The uncomfortably wide range of inferred mass–temperature relations from theory and observations (*cf.,* Table 1 of Pierpaoli et al. (2003), Table 3 of Henry (2004) and Table 1 of Evrard (2004)) is another reason for caution regarding the accuracy of cluster mass estimates.

From Figure 13, it is apparent that implied errors in hydrostatic masses will be model-dependent. For the concordance model with $\sigma_8 = 0.9$, there is little error in normalization at $10^{15} \, h^{-1} \, M_\odot$ after taking the flux bias into account. For the WMAP cosmology, we tuned agreement in the right panel of Figure 13 by choosing $\sigma_8 = 0.85$ and $\sigma_{\ln M} = 0.25$. For a power spectrum normalization of $\sigma_8 = 0.76$, our normalization $\ln L_{15,0}$ is brighter than the RB02 result by a factor of 1.5, indicating that hydrostatic masses are overestimates of the true cluster mass by nearly a factor of 2.

Additional independent estimates of the slope and intercept of the L-M relation would help. Weak lensing analysis of joint X-ray and optical samples is a promising approach that has been applied in a preliminary fashion to clusters in the SDSS Early Data Release (Sheldon et al. 2004). The lensing mass estimates require careful calibration to eliminate the effects of projection (Metzler et al. 2001), but either stacking to acheive spherical symmetry (Johnston 2005) or analysis of mock data from suitably selected simulated clusters (Hennawi & Spergel 2005) can be used to validate procedures used to extract mass estimates from shear maps. Pedersen & Dahle (2006) examine the M-T relation at the high-mass end using lensing masses from 30 clusters, finding a higher normalization than studies using isothermal masses, and finding a power spectrum normalization of $\sigma_8 \sim 0.88$ for $\Omega_m = 0.3$. The large number statistics offered by nearby optical cluster catalogs from SDSS (Bahcall et al. 2003; Miller et al. 2005; Koester 2006) and 2dF (Padilla et al. 2004), when matched with existing and forthcoming archival X-ray data, should ultimately be exploited for this exercise.

5. CONCLUSION

We derive constraints on a model that relates soft X-ray luminosity to halo mass and epoch, $p(L|M,z)$, described as a median power-law relation, $L \propto M^p \rho_c^s(z)$, with log-normal scatter of fixed width $\sigma_{\ln L}$. Convolving this with the mass function of a ΛCDM universe, we perform a likelihood analysis on the counts of galaxy clusters in flux and redshift observed in the REFLEX survey for specific cases of self-similar ($s = 7/6$) and no evolution ($s = 0$). A strong degeneracy between the intercept and scatter in the model means that counts place only an upper limit on the degree of scatter in mass at fixed luminosity $\sigma_{\ln M} < 0.4$.

To improve the estimate of the scatter, we apply additional constraints based on the clustering bias of a volume-limited REFLEX sub-sample and on the intrinsic variance of the observed temperature–luminosity relation. Because the survey probes halo mass scales where the bias is relatively weakly dependent on mass, and because the measured clustering has a substantial uncertainty, the addition of bias has little practical effect on allowed parameters. Using gas dynamical simulations of clusters to probe the inter-relationships of M, T, L, we derive an estimate $\sigma_{\ln M} = 0.43 \pm 0.06$ from the observed scatter in the T-L relation.

After applying these additional constraints, we derive best-fit parameters $p = 1.59 \pm 0.05$, $\sigma_{\ln M} = 0.37 \pm 0.05$, and $\ln L_{15,0} = 1.34 \pm 0.09$ for a concordance cosmology with $\{\Omega_m, \Omega_\Lambda, \sigma_8\} = \{0.3, 0.7, 0.9\}$ and a self-similar evolutionary assumption. The slope and normalization increase, by 2σ and 1σ respectively, under a no evolution assumption. Exploring sensitivity to the assumed (flat-metric) cosmology, we find $L_{15,0} \sim \sigma_8^{-4}$ for fixed Ω_m and $p \sim \Omega_m^{0.5}$ when $\Omega_m \sigma_8^2$ is held fixed. When applying a cosmological model guided by WMAP results, $\Omega_m = 0.24$, $\sigma_8 = 0.85$, and a lower constraint on the scatter, we derive best-fit parameters which include a much higher normalization term, $p = 1.60 \pm 0.05$, $\sigma_{\ln M} = 0.21 \pm 0.06$, $\ln L_{15,0} = 1.92 \pm 0.08$.

Our concordance-model result differs from that determined by RB02 using hydrostatic (isothermal-beta model) mass estimates, being lower in normalization by roughly a factor of two. We show that a bias of this magnitude is expected for the direct L-M relation derived from a flux limited sample, due to a Malquist bias induced by the survey selection process. Correcting for this bias leads to quite good agreement between the two approaches, implying that systematic uncertainties in hydrostatic mass estimates are unlikely to be larger than $\sim 15\%$. To accommodate the change in cosmology preferred by WMAP observations, we offer a compromise solution with slightly elevated σ_8 and lower intrinsic scatter $\sigma_{\ln M}$. Independent approaches to determining the L-M scaling relation, particularly through weak gravitational lensing analysis, should be vigorously pursued.

We anticipate that the approach used here can be fruitfully applied to relations between other observables, such as $X-ray$ temperature or Sunyaev-Zel'dovich decrement, and underlying mass. The coming era of large area, deep cluster surveys, coupled with increasingly detailed numerical simulations, will drive progress, for example, by allowing the evolutionary parameter s to be directly constrained and by enabling investigation of the detailed form of the likelihood $p(L|M, z)$. Possible future refinements for the latter include adding a non-Gaussian component and/or relaxing the assumptions of constant slope and scatter.

<div align="center">APPENDIX</div>

<div align="center">APPENDIX</div>

Consider the case of a power-law mass function at some epoch

$$n(M)\, d\ln M \;=\; n_{15}\, M^{-\gamma}\, d\ln M, \tag{A1}$$

where M is halo mass in units of $10^{15}\, h^{-1}$ M$_\odot$ and n_{15} is the space density at that mass. We show here that convolving the mass function with a log-normal kernel of the form, equation (8), has an effect that is degenerate in normalization and scatter.

For compactness, let $x = \ln M$, $y = \ln L$, $a = \ln L_{15}$, then $\bar{y}(x) = a + p\,x$ and the mass associated with a luminosity y is $\hat{x}(y) = (y - a)/p$. The luminosity function is the convolution

$$n(y)\, dy \;=\; \int dx\, n(x)\, p(y|x)\, dy, \tag{A2}$$

with the kernel a Gaussian of fixed width $\sigma_{\ln L}$

$$p(y|x)\, dy \;=\; \frac{1}{\sqrt{2\pi}\sigma_{\ln L}}\, \exp\left(-(y - \bar{y}(x))^2/2\sigma_{\ln L}{}^2\right) dy. \tag{A3}$$

Linearly transforming the kernel, and using $\sigma_{\ln M} = \sigma_{\ln L}/p$, the luminosity function is

$$n(y)\, dy \;=\; \frac{n_{15}}{\sqrt{2\pi}\, p\, \sigma_{\ln M}} \int dx\, \exp\left(-\gamma x - (x - \hat{x})^2/2\sigma_{\ln M}{}^2\right) dy \tag{A4}$$

Completing the square leads to the result

$$n(y)\, dy \;=\; \frac{n_{15}}{p}\, \exp\left(-\gamma/p[y - (a + \gamma p\sigma_{\ln M}{}^2/2)]\right) dy \tag{A5}$$

which in original notation is

$$n(L)\, d\ln L \;=\; \frac{n_{15}}{p}\, (L/\tilde{L}_{15})^{-\gamma/p}\, d\ln L. \tag{A6}$$

The result is a power-law with slope $-\gamma/p$ and with intercept

$$\ln \tilde{L}_{15} \;=\; \ln L_{15} \;+\; \gamma\, p\, \sigma_{\ln M}{}^2/2. \tag{A7}$$

Since $\tilde{L}_{15}$ is the measurable quantity (call it C), then the observed luminosity function constrains the combination of intercept and scatter

$$\ln L_{15} = C - \frac{\gamma\, p\, \sigma_{\ln M}{}^2}{2} \tag{A8}$$

For values of $\gamma = 3.1$, the local slope of the mass function at $10^{15}\, h^{-1}$ M$_\odot$ for a concordance model, and $p = 1.6$, this expectation is shown as the bold line in the lower right panel of Figure 2.

REFERENCES

Arnaud, M. & Evrard, A. E. 1999, MNRAS, 305, 631
Böhringer, H., et al. 2002, ApJ, 566, 93
Böhringer, H., et al. 2004, A&A, 425, 367
Böhringer, H., et al. 2001, A&A, 369, 826
Bahcall, N. A., et al. 2003, ApJS, 148, 243
Battye, R. A. & Weller, J. 2003, Phys. Rev. D, 68, 083506
Bialek, J. & Evrard, A. E. 2006, in prep
Borgani, S., et al. 2004, MNRAS, 348, 1078
Bryan, G. L. & Norman, M. L. 1998, ApJ, 495, 80
Carlstrom, J. E., Holder, G. P., & Reese, E. D. 2002, ARA&A, 40, 643
Del Popolo, A., Hiotelis, N., & Peñarrubia, J. 2005, ApJ, 628, 76
Ettori, S., Tozzi, P., Borgani, S., & Rosati, P. 2004, A&A, 417, 13
Evrard, A., Metzler, C., & Navarro, J. 1996, ApJ, 469, 494
Evrard, A. E. 1990, ApJ, 363, 349
Evrard, A. E. 2004, in Carnegie Observatories Astrophysics Series, Vol. 3: Clusters of Galaxies: Probes of Cosmological Structure and Galaxy Evolution, ed. J. S. Mulchaey, A. Dressler, and A. Oemler (Cambridge: Cambridge Univ. Press)
Evrard, A. E. & Henry, J. P. 1991, ApJ, 383, 95
Evrard, A. E., et al. 2002, ApJ, 573, 7
Fabian, A. C., Sanders, J. S., Taylor, G. B., Allen, S. W., Crawford, C. S., Johnstone, R. M., & Iwasawa, K. 2006, MNRAS, 366, 417
Fairley, B. W., Jones, L. R., Scharf, C., Ebeling, H., Perlman, E., Horner, D., Wegner, G., & Malkan, M. 2000, MNRAS, 315, 669
Gladders, M. D. & Yee, H. K. C. 2005, ApJS, 157, 1
Haiman, Z., Mohr, J. J., & Holder, G. P. 2001, ApJ, 553, 545
Hennawi, J. F. & Spergel, D. N. 2005, ApJ, 624, 59
Henry, J. P. 2004, ApJ, 609, 603
Holder, G. P., Mohr, J. J., Carlstrom, J. E., Evrard, A. E., & Leitch, E. M. 2000, ApJ, 544, 629
Horner, D. J. 2001, PhD thesis, University of Maryland, College Park
Hu, W. & Kravtsov, A. V. 2003a, ApJ, 584, 702
—. 2003b, ApJ, 584, 702
Ikebe, Y., Reiprich, T. H., Böhringer, H., Tanaka, Y., & Kitayama, T. 2002, A&A, 383, 773
Jenkins, A., Frenk, C. S., White, S. D. M., Colberg, J. M., Cole, S., Evrard, A. E., Couchman, H. M. P., & Yoshida, N. 2001, MNRAS, 321, 372
Johnston, D. E. *et al.*. 2005, MNRAS, in press, astro-ph/0503282
Kaiser, N. 1986, MNRAS, 222, 323
Koester, B. *et al.*. 2006, in prep.
Kosowsky, A. 2003, New Astronomy Review, 47, 939
Levine, E. S., Schulz, A. E., & White, M. 2002, ApJ, 577, 569
Lima, M. & Hu, W. 2004, Phys. Rev. D, 70, 043504
—. 2005, Phys. Rev. D, 72, 043006
Loh, M., et al. 2005, American Astronomical Society Meeting Abstracts, 207,
Majumdar, S. & Mohr, J. J. 2003, ApJ, 585, 603
Mathiesen, B. F. & Evrard, A. E. 2001a, ApJ, 546, 100
—. 2001b, ApJ, 546, 100
Maughan, B., Jones, L., Ebeling, H., & Scharf, C. 2005, MNRAS, in press, astro-ph/0503455
Mazzotta, P., Edge, A. C., & Markevitch, M. 2003, ApJ, 596, 190
Metzler, C. A., White, M., & Loken, C. 2001, ApJ, 547, 560
Miller, C. J., et al. 2005, AJ, 130, 968
Mohr, J. J., Mathiesen, B., & Evrard, A. E. 1999, ApJ, 517, 627
Mullis, C. R., Rosati, P., Lamer, G., Böhringer, H., Schwope, A., Schuecker, P., & Fassbender, R. 2005, ApJ, 623, L85
Mushotzky, R. F. & Scharf, C. A. 1997, ApJ, 482, L13
Navarro, J. F., Frenk, C. S., & White, S. D. M. 1995, MNRAS, 275, 56
Novicki, M. C., Sornig, M., & Henry, J. P. 2002, AJ, 124, 2413
O'Hara, T. B., Mohr, J. J., Bialek, J. J., & Evrard, A. E. 2006, ApJ, 639, 64
Padilla, N. D., et al. 2004, MNRAS, 352, 211
Pedersen, K. & Dahle, H. 2006, arXiv:astro-ph/0603260
Pen, U.-L. 1999, ApJS, 120, 49
Pierpaoli, E., Borgani, S., Scott, D., & White, M. 2003, MNRAS, 342, 163
Pierpaoli, E., Scott, D., & White, M. 2001, MNRAS, 325, 77
Rasia, E., et al. 2006, arXiv:astro-ph/0602434
Rasia, E., Tormen, G., & Moscardini, L. 2004, MNRAS, 351, 237
Reed, D., Gardner, J., Quinn, T., Stadel, J., Fardal, M., Lake, G., & Governato, F. 2003, MNRAS, 346, 565
Reiprich, T. H. 2006, arXiv:astro-ph/0605009
Reiprich, T. H. & Böhringer, H. 2002, ApJ, 567, 716
Ricker, P. M. & Sarazin, C. L. 2001, ApJ, 561, 621
Romer, A. K., et al. 2000, ApJS, 126, 209
Rosati, P., della Ceca, R., Norman, C., & Giacconi, R. 1998, ApJ, 492, L21+
Rowley, D. R., Thomas, P. A., & Kay, S. T. 2004, MNRAS, 352, 508
Ruhl, J., et al. 2004, Astronomical Structures and Mechanisms Technology, Proceedings of the SPIE, 5498, 11 (2004)
Schindler, S. 1996, A&A, 305, 756
Schuecker, P., et al. 2001, A&A, 368, 86
Schuecker, P., Caldwell, R. R., Böhringer, H., Collins, C. A., Guzzo, L., & Weinberg, N. N. 2003, A&A, 402, 53
Schwan, D., et al. 2003, New Astronomy Review, 47, 933
Seljak, U. & Zaldarriaga, M. 1996, ApJ, 469, 437
Sheldon, E. S., et al. 2004, AJ, 127, 2544
Sheth, R. K. & Tormen, G. 1999, MNRAS, 308, 119
Spergel, D. N., et al. 2006, arXiv:astro-ph/0603449
Stanford, S. A., et al. 2005, ApJ, 634, L129
Vikhlinin, A., Markevitch, M., Murray, S. S., Jones, C., Forman, W., & Van Speybroeck, L. 2005, ApJ, 628, 655
Wang, L. & Steinhardt, P. J. 1998, ApJ, 508, 483
Wang, S., Khoury, J., Haiman, Z., & May, M. 2004, Phys. Rev. D, 70, 123008
Warren, M. S., Abazajian, K., Holz, D. E., & Teodoro, L. 2005, arXiv:astro-ph/0506395